國立交通大學

物　　理　　研　　究　　所

碩　士　論　文

# 光電倍增管反應模擬研究及香港亞伯丁宇宙線實驗校正

# Monte Carlo Studies of Photomultiplier Tube Responses and Calibrations in Aberdeen Cosmic Ray Experiment

研　究　生：陳志榮

指導教授：林貴林 教授

共同指導：王正祥 教授

中　華　民　國　九　十　九　年　七　月

# 光電倍增管反應模擬研究及香港亞伯丁宇宙線實驗校正

# Monte Carlo Studies of Photomultiplier Tube Responses and Calibrations in Aberdeen Cosmic Ray Experiment


研 究 生：陳志榮　　Student: Chih-Jung Chen

指導教授：林貴林　　Advisor: Guey-Lin Lin

共同指導：王正祥　　Co-Advisor: Chung-Hsiang Wang


國立交通大學

物理研究所

碩士論文

A Thesis

Submitted to Institute of Physics

National Chiao Tung University

in Partial Fulfillment of the Requirements

for the Degree of

Master

in

Physics

July, 2010

Hsinchu City, Taiwan, Republic of China

中華民國九十九年七月

# 光電倍增管反應模擬研究及香港亞伯丁宇宙線實驗校正

研究生：陳志榮　　指導教授：林貴林
共同指導：王正祥

國立交通大學物理研究所

## 摘　　要

近年來，液態閃爍體粒子探測器被廣泛應用於許多大型粒子偵測器當中，例如大亞灣計畫以及香港亞伯丁宇宙線偵測器。此類探測器多半以光電倍增管作爲訊號採集以及放大，其校正與監控對實驗數據的可信度有很重要的影響。Bellamy的研究團隊於1994年發表了一篇以反應函數擬合從探測器得到的能譜來監控光電倍增管的方法[1]，該反應函數包含了光電倍增管大部份重要的變數，每一項變數剛好對應到一項光電倍增管的物理特性。然而，對於一些比較複雜的探測器系統，反應函數以不同起始值擬合相同能譜，會給出不同的結果，我們認爲該函數因參數較多，在擬合上本會產生許多解，只是正確的解該落在哪我們並不清楚。所以，我們使用蒙地卡羅模擬來確認不同起始值對擬合結果的影響，進而歸類出較符合物理的解。本論文將探討反應函數，蒙地卡羅模擬方法，以及兩點關於香港亞伯丁探測器的應用。

# Monte Carlo Studies of Photomultiplier Tube Responses and Calibrations in Aberdeen Cosmic Ray Experiment

Student: Chih-Jung Chen

Advisor: Guey-Lin Lin

Co-Advisor: Chung-Hsiang Wang

Submitted to Institute of Physics

National Chiao Tung University

## ABSTRACT

Recently, scintillation detectors are extensively used in many projects with particle detector such as Dayabay and Aberdeen. Usually in such detectors, photomultiplier tubes (PMT) are used for the detection of light. The paper by Bellamy *et al.* [1] gives a good tool, i.e., PMT response function, to simplify the calibration process. The response function already considers almost every variable of spectrometric channel from PMT. Each variable is directly proportional to one of PMT's parameters. However in some case, using response function to fit spectra from the same system could give different results especially when initial values taken in the fitting are varied. Our conclusion is that there are many local minima in the fitting. Monte Carlo simulation is a good scheme to understand the issue of multiple local minima. In this thesis, we shall introduce the response function, and use Monte Carlo simulation to deal with local minima. At last, we shall present two applications to Aberdeen cosmic ray experiment.

# 致　謝

感謝指導教授林貴林老師在研究方面的指引與教導。
感謝共同指導王正祥老師在高能實驗方面的教導。
感謝聯合大學黃明輝老師提醒我觀念上的錯誤。
感謝台灣大學熊怡老師在大亞灣的幫助以及教導。
感謝香港大學及香港中文大學的亞伯丁實驗團隊給予的技術協助。

最後，感謝整個Group兩年來的熱情陪伴！

# Contents

# List of Figures

# List of Tables



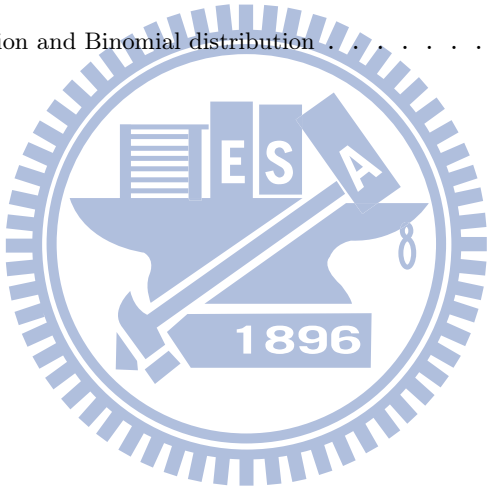

# Introduction

Recently, scintillation detectors are extensively used in many project with particle detector such as Dayabay and Aberdeen. Usually in such detectors, photomultiplier tubes (PMT) are used for the detection of light. In detectors of this type there exists not only an intrinsic spread in characteristic parameters among different PMTs, but also time dependence of parameters of a given PMT. Therefore a systematic calibration and monitoring of the PMT based spectrometric channels is an important part of the experimental setups employing scintillation detectors.

Usually we calibrate our system with irradiation sources (such as $^{60}$Co, $^{137}$Cs, etc.) whose energy spectra and characteristic peaks have been measured quite accurately in many experiments. It is efficient, but not always accurate especially in a complicated system, for example, neutron detector in Aberdeen project which has 16 PMTs with different gains and different trigger voltages. To make sure 16 characteristic peaks are at the same channel position, we need PMTs' gain curve first. Unfortunately, irradiation source can only give *relative* gain, not absolute one, so we need a standard measurement by other source whose light intensity and frequency can be controlled, such as LED or laser, so more diverse environments and more variables can be considered.

The paper by Bellamy *et al.* [1] gives a good tool, i.e., photomultiplier response function, to simplify calibration process. The response function already considers almost every variable of spectrometric channel (ADC channel) from PMT. Each variable is directly proportional to one of PMT's parameters. In that work, they present a method for the absolute calibration of spectrometric channels based on a statistical analysis of the PMT spectra from a pulsed light source. However this paper does not discuss complications in actual experiments mentioned above. Actually in some case, using response function to fit spectra from the same system could give different results especially when initial values chosen for the fitting are varied. Some parameters in function have high correlations and are sensitive to the fitting range and the initial values. We first thought that it was caused by system fluctuations. However we pick up one spectrum and fit it several times, we still obtain different results. Our conclusion is that there are many local minima for the fitting. Each local minimum has its statistical significance. However, only one group of parameters could correspond to the real world.

Monte Carlo simulation is a good scheme to understand the issue of multiple local minima once we know the basic properties of our detector and system. The main idea is to use random number generator to generate many different histograms (or say ADC channel, spectrometric channel, etc.) whose behavior follows the same response function. We then fit these histograms and identify all possible local minima. We will present details later in this thesis.

# Chapter 1

# Photomultiplier tubes

In this chapter, we discuss some basic properties of photomultiplier tubes. We do not touch upon the design details such as the material of cathodes, efficiency of different tube geometry, etc. We simply focus on the general formula and properties of photomultiplier tubes.

## Basic principles of photomultiplier tubes

A photomultiplier tube is a vacuum tube consisting of an input window, a photocathode, focusing electrodes, an electron multiplier and an anode usually sealed into an evacuated glass tube. Figure 4.2 shows the schematic structure of a photomultiplier tube.

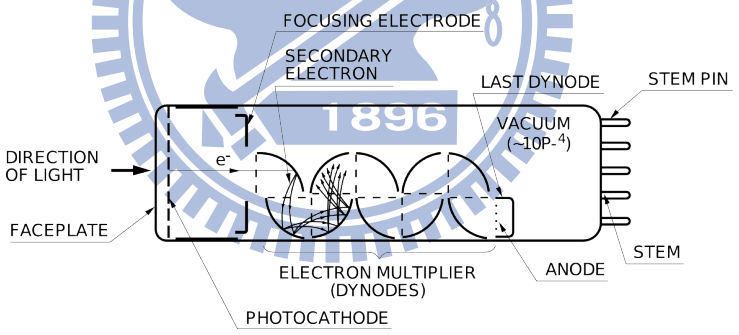


Figure 1.1: Structure of a photomultiplier tube

Photon passes through the input window and hits (or excites) electrons out in the photocathode by photoelectric effect. These electrons are referred to as photoelectrons. Photoelectrons are accelerated and focused by the focusing electrode onto the first dynode where they are multiplied by means of secondary electron emissions. This secondary emissions are repeated at each of the successive dynodes. Then, the multiplied secondary electrons emitted from the last dynode are finally collected by the anode. The output is a current, not a voltage. Hence we need to connect a proper resistance to make a potential drop if we want to take the signal by a scope. This section describes the principle of photoelectron emissions, electron trajectory, and the design of electron multipliers.

### Photoelectron emission

Photoelectric conversion is broadly classified into external photoelectric effects by which photoelectrons are emitted into the vacuum from a material and internal photoelectric effects by which photoelectrons

are excited into the conduction band of a material. The photocathode has the former effect and the latter are represented by the photoconductive or photovoltaic effect [7].

## Electron trajectory

In order to collect photoelectrons and secondary electrons efficiently on a dynode and also to minimize the electron transit time spread, electrode design must be optimized through an analysis of the electron trajectory [7].

Electron movement in a photomultiplier tube is influenced by the electric field which is dominated by the electrode configuration and the voltage applied to the electrode. Numerical analysis of the electron trajectory using high-speed, large-capacity computers have come into use. This method divides the area to be analyzed into a grid-like pattern to give boundary conditions, and obtains an approximation by repeating computations until the error converges to a certain level. By solving the equation for motion based on the potential distribution obtained using this method, the electron trajectory can be predicted [7].

## Electron multiplier

As stated above, the potential distribution and electrode structure of a photomultiplier tube is designed to provide optimum performance. Photoelectrons emitted from the photocathode are multiplied from the first dynode till the last dynode (up to 19 dynodes), with current amplification ranging from 10 to as much as $10^8$ times, and are finally sent to the anode [7].

When a primary electron with initial energy $E_p$ strikes the surface of a dynode, $\delta$ secondary electrons are emitted. This $\delta$, the number of secondary electrons per primary electron, is called the secondary emission ratio. Ideally, the current amplification or gain of a photomultiplier tube having the number of dynode stages $n$ and the average secondary emission ratio $\delta$ per stage will be $\delta^n$ [7].

## Anode

The anode of a photomultiplier tube is an electrode that collects secondary electrons multiplied in the cascade process through multi-stage dynodes and outputs the electron current to an external circuit [7].

# Chapter 2

# Photomultiplier tube response function

In this chapter, we introduce the model for photomultiplier response which was constructed by E.H. Bellamy *et al.* [1]. And applications of such a model on LED spectra and irradiation source spectra. Weak light source is the basis for the response function. LED intensity is weak enough and controllable. So that its spectra can be understood by the response function.

## A model of photomultiplier response

Photomultiplier response function consists of photon conversion, electron collection, amplification and background noise. Photoconversion and electron collection are actually equivalent. They can transform to each other by multiplying or dividing quantum efficiency. Amplification is a spectrum of one photon transforming to current which depends on PMT's reaction and dynode numbers. The background noise is just a general assumption.

### Photoconversion and electron collection

Let us suppose that we have a source of light pulse with controllable frequency and intensity. The flux of photons incident on the PMT photocathode produces photoelectrons via the photoelectric effect. Under real circumstances, the number of photons hitting the photocathode and becoming photoelectrons is not a constant but follows binomial distribution

$$P(n) = \frac{N!}{n!(N-n)!}(1-p)^{N-n}p^n \tag{2.1}$$

where $p$ is the probability of photon being caught by PMT and becoming a photoelectron collected by the dynode system, and $N$ is total emitted photon. The size of PMT's window and quantum efficiency of photocathode determine $p$. As we mention above, weak intensity is the basis for the response function, so only a fraction of the emitted photons is picked up by the PMT. If the pulse source has operated a while, one can imagine that huge number of photons, referred to as $N$, has been emitted. In the case that $N \gg 1$, the binomial distribution approaches to Poisson distribution, i.e.,

$$\begin{aligned} P(n) &\simeq \lim_{N\gg 1} \frac{N!}{n!(N-n)!}(1-p)^{N-n}p^n \\ &\simeq \lim_{N\gg 1} \frac{N!}{n!(N-n)!}\left(1-\frac{Np}{N}\right)^{N-n}\frac{(Np)^n}{N^n} \\ &\simeq \frac{\mu^n}{n!}e^{-\mu} \end{aligned} \tag{2.2}$$

where $\mu = Np$ [1]. For more details, please refer to Appendix A

In the real circumstance, we usually allow few photons hitting a PMT. A PMT always possess extremely high current gain and rapid reaction time. With a huge number of photons passing through the PMT, a sharp current will be induced in the electronic system. This is like a lightning hitting the system and damaging it. So we usually decrease $p$ to a small value (near zero) by controlling intensity of pulse source or distance between source and PMT.

We would like to note that $\mu$ is a parameter characterizing not only the photocathode quantum efficiency as mentioned above, but also the light source intensity and electron collection efficiency of the PMTs dynode system. Thus $\mu$, the mean number of collected photoelectrons, is determined by the mean number of photons hitting the photocathode, the photocathode quantum efficiency, and the collection efficiency of the dynode system [1].

## Amplification

Let us imagine an ideal condition that there is only one photoelectron hitting first dynode and the dynode produce $g_1$ electrons ($g_1 > 1$), which is the so called secondary electron emission. These electrons then hit the second dynode in a binomial process which produces $n_1 g_2$ electrons. Again, $n_1 g_2$ electrons hit the third dynode in a binomial process which produces $n_2 g_3$ electrons, and so on. Here, $n_i$ is the electron number picked up by each dynode and $g_i$ is each dynode's gain coefficient. The groups of electrons between dynodes are independent because the number of electrons in one group was determined by one dynode at each stage. Therefore, the distribution of $K$ events are mainly determined by the final stage. This gives again, a binomial distribution

$$G(x) = \frac{K!}{x!(K-x)!}(1-\rho)^{K-x}\rho^x \tag{2.3}$$

where $\rho$ is the probability of an electron in the final dynode being exited to the escape energy, $K$ is total valence electrons on the dynode. Likely, $K$ is incredible huge ($> 10^6$) and $\rho$ almost remains the same for each valence electron. In this case, a binomial distribution approaches to a Gaussian (see Appendix B)

$$\begin{aligned}\lim_{K\gg 1} G(x) &= \lim_{K\gg 1} \frac{K!}{x!(K-x)!}(1-\rho)^{K-x}\rho^x \\ &\simeq \frac{1}{\sqrt{2\pi}}\frac{1}{\sigma_1}\exp\left[-\frac{(x-Q_1)^2}{2\sigma_1^2}\right]\end{aligned} \tag{2.4}$$

where $x$ is the charge variable, $Q_1 = K\rho$ is the average charge at the PMT output when one electron is collected by the first dynode, $\sigma_1 = \sqrt{K\rho(1-\rho)}$ is the corresponding standard deviation of the charge distribution [1].

Of course $Q_1$ can be expressed through the PMT gain coefficient $g$ and elementary charge $e$, as $Q_1 = eg$. The PMT output charge distribution in the case that more than one photoelectron are collected by the first dynode can be derived from formula (2.4) if one assumes that the amplification processes of the charges initiated by different photoelectrons are mutually independent. In this case the charge distribution due to $n$ photoelectrons, is a convolution of $n$ one-electron cases [1]

$$G_n(x) = \frac{1}{\sqrt{2\pi n}}\frac{1}{\sigma_1}\exp\left[-\frac{(x-nQ_1)^2}{2n\sigma_1^2}\right] \tag{2.5}$$

Note that this distribution has a correct limit for $n \to 0$

$$G_0(x) = \delta(x) \tag{2.6}$$

where $\delta(x)$ is the delta function. This condition ensures that the amplification of an input zero charge results in zero charge at the output [1].

It is important to note that expression (2.5) is correct provided the probability of a photoelectron missing the first dynode and being captured by one of the subsequent dynodes is negligible.

The response of an ideal noiseless PMT can now be readily found. In this case the resulting output signal is simply a convolution of the distributions (2.2) and (2.5)

$$\begin{aligned} S_{\text{ideal}}(x) &= P(n;\mu) \otimes G_n(x) \\ &= \sum_{n=0}^{\infty} \frac{\mu^n e^{\mu}}{n!} \frac{1}{\sigma_1 \sqrt{2\pi n}} \exp\left[ -\frac{(x - nQ_1)^2}{2n\sigma_1^2} \right] \end{aligned} \tag{2.7}$$

with the above mentioned limit condition for the limit $n = 0$ [1].

## Background processes

Even though we set up the PMT system in a completely dark room (with no light source), there is still a small amount of current flowing in a PMT. This output signal is called the dark current or noise. The possible source of dark currents are: thermionic emission current from the photocathode and dynodes; leakage current (ohmic leakage) between the anode and other electrodes inside the tube and/or between the anode pin and other pins on the bulb stem; electronic system such as high voltage supply, discriminator, fan-in-fan-out; noise current caused by cosmic rays, radiation from radioisotopes contained in the glass envelopes and environmental gamma rays. In addition to the above, there are still other sources of dark current such as field emission current, ionization current, etc. These noises can be subtracted by controlling electronic system such as, data acquisition (DAQ) system. For example, giving a proper high voltage can decrease emission current quite a lot while opening appropriate time window can avoid ionization currents.

### Thermionic emission

Since the photocathode and dynode surfaces are composed of materials with very low work functions, they emit thermionic electrons even at room temperatures. We can regard those escaped electrons as being excited by thermal effect to an energy level which is far away from Fermi surface. In this case, we can treat the energy distribution as Fermi-Dirac distribution

$$f(\varepsilon) = \frac{1}{\exp\left[ (\varepsilon - \psi)/k_B T \right] + 1} \tag{2.8}$$

where

$\varepsilon$ : energy of electron

$\psi$ : work function and chemical potential

$k_B$ : Boltzmann constant

$T$ : absolute temperature

Normally, we operate PMT in room temperature, $300K$ for example (about $27°C$), so that $k_B T$ is about 1/38.681 eV. Work function and chemical potential is usually several electron volts, which implies $\exp\left[ (\varepsilon - \psi)/k_B T \right] \gg 1$. Hence Fermi-Dirac distribution can be approximated as

$$\frac{1}{\exp\left[ (\varepsilon - \psi)/k_B T \right] + 1} \simeq \exp\left[ -\frac{\varepsilon - \psi}{k_B T} \right] \tag{2.9}$$

With appropriate normalization, we have

$$f(x') = ae^{-ax'} \tag{2.10}$$

where $x' = \varepsilon - \psi$ and $a = 1/(k_B T)$. The implication of this result will be discussed later.

**Leakage current**

Photomultiplier tubes are operated at high voltages from 500 up to 3000 volts which are provided by the voltage supply. A leakage current may be generated between the anode and the last dynode inside a tube. It may also be caused by imperfect insulation of the glass stem and base, and between the socket anode pin and other pins [7]. A leakage will give a DC output if we observe the signal on the scope. Therefore every signal has a voltage shift called *Pedestal*. Corresponding to the spectrum, it gives a Gaussian distribution with narrow width, not a delta function (but almost)

$$g(x) = \frac{1}{\sigma_0\sqrt{2\pi}} \exp\left(-\frac{x^2}{2\sigma_0^2}\right) \tag{2.11}$$

where $\sigma_0$ is the fluctuation of the high voltage [1].

There are two reasons for the fluctuation. One reason is that there is no high voltage supply which could give a *perfectly* DC voltage without any fluctuation. Usually, a voltage supply is composed of several different and complicated electronic functions including RC, LC, and RLC circuits. Such circuits give the system an oscillation current which can be reduced but not be subtracted. This oscillation is usually regular and has a long period. So the spectrum is a Gaussian, with a width reflecting the high voltage stability.

Another reason for the fluctuation is the input resistance. A voltage crossing a component such as PMT gives a current and heats the resistance in it. Usually, the resistance is proportional to the temperature. Hence it decreases the currents. As a result, the work on the component is decreased which then lowers the temperature. Once the resistance is lowered, currents rise up. Repeating the above process gives oscillation again.

**Electronic system**

Typically, PMT operates with a DAQ system such as an oscilloscope. There are several basic functions in the scope such as trigger level and trigger condition. Trigger level means the input signal needs to reach some voltage so that the scope could display it. Trigger condition is a function which provided random trigger, channel dependent trigger, external trigger, etc. For example, trigger level provides a simple way to filter the noise such as leakage current. If the peak of noise signal is lower than some value, we can set this voltage as trigger level so that the noise spectrum could be subtracted. This behavior will refresh the final spectrometric channel. The probability of signal recording is related to the charge of incident photoelectrons which is not a constant. This part is hard to calculate. If we want to use the response function to calibrate the system, trigger level should be set into a value lower than the pedestal.

**Noise current caused by cosmic rays**

Many types of cosmic particles fall on the Earth constantly. Among them, muons can be a major source of photomultiplier tube noise. When muons pass through the glass envelope, Cherenkov radiation may occur, releasing a large number of photons. In addition, most glasses contain potassium oxide which also contains a small amount of the radioactive element $^{40}$K. $^{40}$K may emit beta rays and result in a noise. Furthermore, environmental gamma rays emitted from radioisotopes contained in buildings could

be another source of noise. However, because these dark noises occur much less frequently, they are negligible except for applications such as liquid scintillation counting where the number of signal counts is exceptionally small [7].

The effect of these processes in the case that some primary photoelectrons $n \geq 1$ are emitted will be discussed later. When no primary photoelectron is emitted ($n = 0$, with probability $e^{-\mu}$), the totality of the signal will be due to these backgrounds. If we call $w$ the probability that, within these events, a background signal of thermionic emission can occur, we can parameterize the background as [1]

$$B(x) = \frac{(1-w)}{\sigma_0\sqrt{2\pi}} \exp\left(-\frac{x^2}{2\sigma_0^2}\right) + w\theta(x)\,\alpha e^{-\alpha x} \tag{2.12}$$

where $\sigma_0$ is the standard deviation of the leakage current distribution, $w$ is the probability that a measured signal is accompanied by a thermionic emission process, $\alpha$ is the coefficient of the exponential decrease of thermionic emission and [1]

$$\theta(x) = \begin{cases} 0 & x < 0 \\ 1 & x \geq 0 \end{cases} \tag{2.13}$$

is the step function. Notice that $x'$ and $a$ in (2.10) is not the same as $x$ and $\alpha$ here. We assume that the distribution from thermionic emission through dynode system is similar to thermionic emission only. So we just parametrize (2.10) and using the dimensionless variables $x$ and $\alpha$ here.

## The realistic response function of the photomultiplier

Taking into account the ideal PMT spectrum (2.5) and the background charge distribution (2.12) we find the realistic PMT spectrum as the convolution:

$$\begin{aligned} S_{\text{real}}(x) &= \int S_{\text{ideal}}(y)\, B(x-y)\, \mathrm{d}y \\ &= \sum_{n=0}^{\infty} \frac{\mu^n e^{-\mu}}{n!} \left[(1-w)\,\mathcal{G}_n(x-Q_0) + w I_{G_n\otimes E}(x-Q_0)\right] \end{aligned} \tag{2.14}$$

with

$$\mathcal{G}_n(x-Q_0) = \frac{1-w}{\sigma_n\sqrt{2\pi}} \exp\left[-\frac{(x-Q_n)^2}{2\sigma_n^2}\right] \tag{2.15}$$

$$I_{G_n\otimes E}(x-Q_0) = \int_{Q_0}^{x} G_n(y-Q_0)\,\alpha \exp\left[-\alpha(x-y)\right] \mathrm{d}y \tag{2.16}$$

$$\begin{aligned} &= \left[\operatorname{erf}\left(\frac{x-Q_n-n\sigma_1^2\alpha}{\sigma_1\sqrt{2n}}\right) + \operatorname{erf}\left(\frac{|\,Q_0-Q_n-n\sigma_1^2\alpha\,|}{\sigma_1\sqrt{2n}}\right)\right] \\ &\times \frac{\alpha}{2} \exp\left[-\alpha\left(x-Q_n-\frac{n\sigma_1^2\alpha}{2}\right)\right] \end{aligned} \tag{2.17}$$

$$\begin{aligned} Q_n &= Q_0 + nQ_1 \\ \sigma_n &= \sqrt{\sigma_0^2 + n\sigma_1^2} \\ \Theta(z) &= \begin{cases} 1 & z \geq 0 \\ -1 & z < 0 \end{cases} \end{aligned} \tag{2.18}$$

where $Q_0$ is the pedestal and $\mathrm{erf}(x)$ is the error function.

The meaning of other parameters are the same as those in (2.2), (2.5) and (2.12). $\mathcal{G}_n(x)$ is now a convolution of the ideal PMT $n$ photoelectrons charge distribution (2.7) with the Gaussian part of background (2.12). The standard deviation associated with $\mathcal{G}_n(x)$ is $\sqrt{\sigma_0^2 + n\sigma_1^2}$. In the zero photoelectron case, $\mathcal{G}_n(x - Q_0)$ is not a delta function any more, but a Gaussian with standard deviation $\sigma_0$. Hence, $I_{G_n \otimes E}$ is reduced to $\alpha \exp[-\alpha(x - Q_0)]$.

In summary, we note that the response function (2.14) of a real PMT contains seven free parameters. Two of them $Q_0$ and $\sigma_0$ define the pedestal. Two others, $w$ and $\alpha$ describe the background, and the remaining three parameters $Q_1$, $\sigma_1$ and $\mu$ describe the spectrum of the real signal. Of these three parameters, $\mu$ is proportional to the intensity of the light source, and two remaining ones $Q_1$, $\sigma_1$ characterize the amplification process of the PMT dynode system [1].

The fact that the intensity of the light source can be separated from the amplification process plays a crucial role in the calibration and monitoring of a spectrometric channel. If we are able to deconvolute the spectrum indicated in (2.14), i.e. to find its parameters, we can use parameter $Q_1$ as a calibration unit as well as a parameter for checking the stability of PMT operation. The absolute PMT gain coefficient is also given by $Q_1$. The stability of the photoelectron signal will be monitored by $\mu$.

# Applications

In this section, we shall present two typical examples, one is LED light source and another is irradiation source. LED spectra were directly taken from E.H.Bellamy's paper [1], and irradiation source spectra were from Aberdeen project.

## LED spectra

The developed analytical method was applied to the calibration of a few PMTs employing a low intensity pulsed light source. The block diagram for the calibration measurement is shown in Figure 2.1. A LED was used as a pulsed light source. The LED was driven by a pulse generator (GEN) with a short pulse width ($\leq 10$ ns). An optical fiber was used to transmit light from the LED to the PMT so as to eliminate electrical noise from the generator. The photon intensity incident on the photocathode was tuned by changing the amplitude of the supply voltage to the LED. The analog output signal from the PMT was measured by an ADC (LeCroy 2249A). The width of the gate signal was 80 ns.

The measurements were performed with different light source intensities, applied voltages to the PMT, and in types of PMT used. Most measurements were carried out in Ref [1] using an EMI-9814B photomultiplier. We do not use this type of PMT. The main idea of this subsection is just a demonstration of analytical method. Pulse height spectra were de-convoluted by means of a program based on the Minuit2 Minimization Package using the PMT response function (2.14) as the fitting function. Results of spectral fittings are summarized in the Figures 2.2.

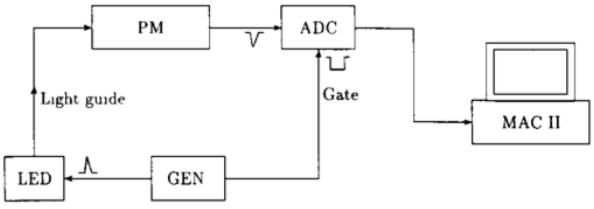


Figure 2.1: Block scheme of the calibration setup [1].

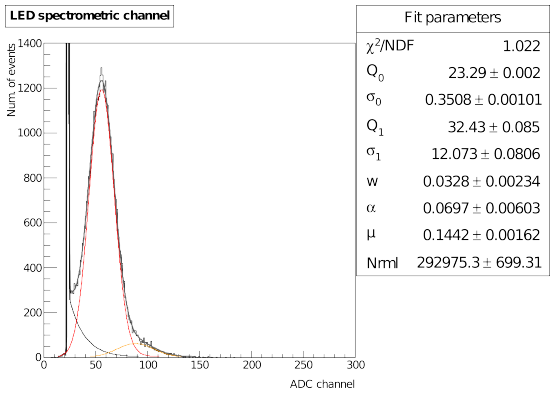


(a) $\mu \sim 0.14$ average photoelectrons during whole operating times

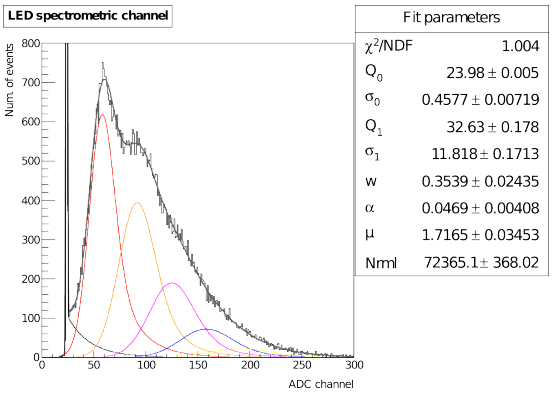


(b) $\mu \sim 1.72$ average photoelectrons

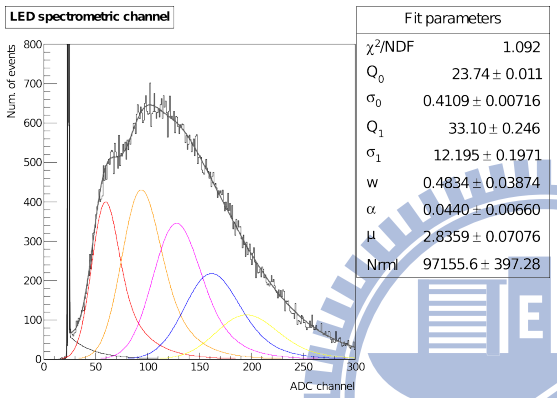


(c) $\mu \sim 2.84$ average photoelectrons

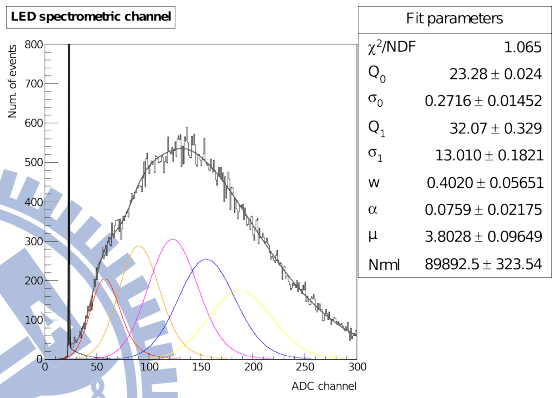


(d) $\mu \sim 3.80$ average photoelectrons

Figure 2.2: LED spectra at constant voltage and different intensities of light source [1].

As mentioned earlier, $\mu$ and $Q_n$ stand for average photoelectron and average output charge with $n$ photoelectrons respectively. Therefore, $Q_1$ is proportional to PMT gain $g$ such that

$$g = \frac{Q_1}{[\text{electron charge (Coulomb)}]\,[\text{QDC sensitivity (channel/Coulomb)}]} \tag{2.19}$$

## Irradiation source spectra

Different from the last section, irradiation source can not be controlled. Hence the experiment setup was less trivial. As discussed before, background signal gives rise to a non-negligible contribution, especially in $n = 0$ term. The usual random trigger would miss such a leakage current at $n = 0$ term. Hence a design of simultaneously taking signals and pedestal is required. In the next example, we shall discuss the surface experiment of Aberdeen project.

Below is the setup scheme. First, four PMTs are situated at each corner of the nine cubic meters cube on the bottom, so that PMTs form a square and each PMT has about a three- meter distance from the nearest two PMTs. Next, a irradiation source is placed at the center of PMT square. We uses $^{60}$Co as the irradiation source. Finally, we choose the 3 out of 4 trigger condition which means if any three PMTs have signal reaching trigger voltage (trigger level) in the same time window (or said, at the same time), DAQ system will record this event from four PMTs no mater it was dark current or signal. Under this

circumstance, output spectrum have both $n = 0$ and $n > 0$ terms.

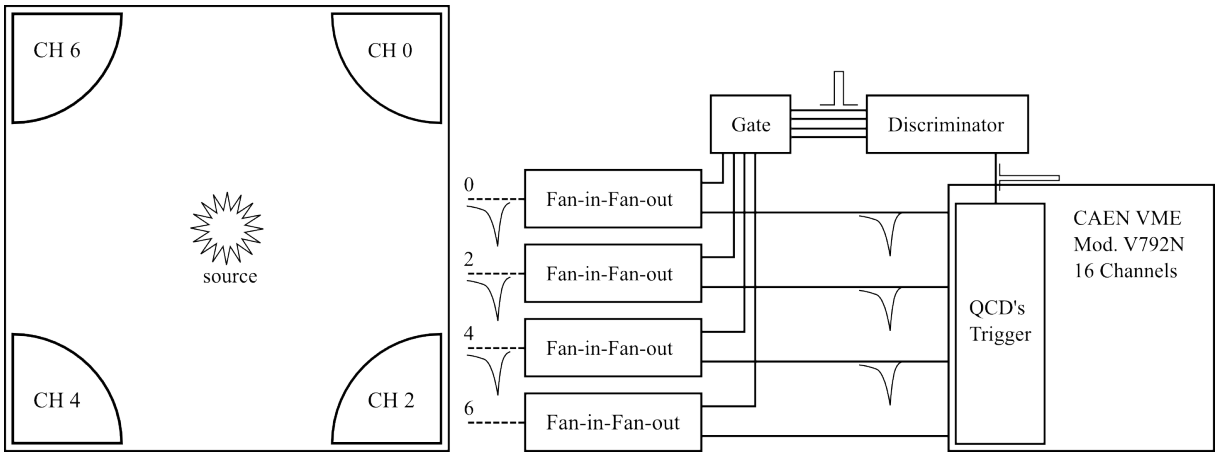


Figure 2.3: The block diagram of surface experiment.

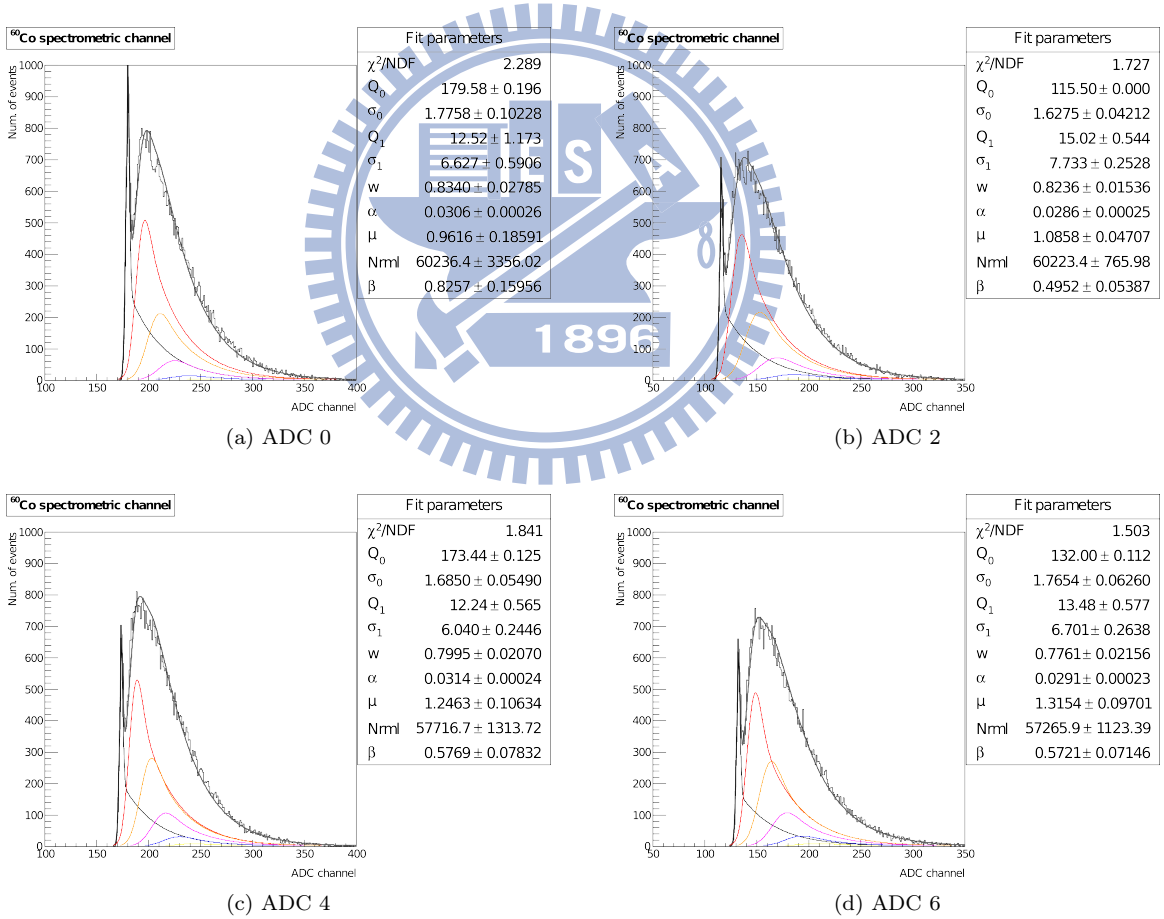


(a) ADC 0 (b) ADC 2

(c) ADC 4 (d) ADC 6

Figure 2.4: $^{60}$Co gamma spectra. CH 0, CH 2, CH 4 and CH 6 correspond to each QDC Channel respectively.

Figure 2.4 shows the fitting result. Notice that the response function used here differs slightly from eq (2.14). Because Gamma source emits photon randomly, we can not make sure that the coming photons each time can trigger only 3 PMTs without any 4 out of 4 event. Hence, the probability of pedestal (or say, leakage current) was underestimated. To deal with this problem, we add a coefficient $\beta$ at the pedestal part

$$S_{\text{real}}(x) = e^{-\mu}\left[\frac{\beta(1-w)}{\sigma_0\sqrt{2\pi}}\exp\left(-\frac{(x-Q_0)^2}{2\sigma_0^2}\right) + w\theta(x-Q_0)\,\alpha e^{-\alpha x}\right] \tag{2.20}$$
$$+\sum_{n=1}^{\infty}\frac{\mu^n e^{-\mu}}{n!}\left[(1-w)\,\mathcal{G}_n(x-Q_0) + wI_{G_n\otimes E}(x-Q_0)\right]$$

# Chapter 3

# Simulation on PMT response function

## Motivation

Response function seems to work quite well in both pulse light case and irradiation source case. As we have seen, there are totally seven parameters (not including $\beta$ and normalization factor), which are not independent. In the subsection *Background processes*, one can compare $a$ and $\alpha$ in (2.10) and (2.12) respectively. Although $a$ is just a simple function of temperature, the resulting parameter $\alpha$ after convoluting to each dynode is not only a function of $T$ but also contains information about gain, electron collection, and high voltage. Other parameters such as $w$ and $\sigma_1$ have similar situations.

In LED case, experimental variables can be controlled in an ideal way so that the fitting method could produce stable results. However, this does not apply to our interested case. We like to construct a good algorithm based on mathematical modeling which can provide a reference for detector calibrations using a small set of data. In the case of irradiation source, the situation was more complicated than LED. First, original response function (2.14) is only a good description for pulse light case. It is however an *approximation* in the irradiation case since such a source has its own special spectrum or probability density function. Secondly, ADC channel depends on the PMT position. For instance, in 3 out of 4 case as we have mentioned before, $\beta$ is proportional to the distance between source and PMT. Because the role of $\beta$ in the response function is similar to $w$ (both determine function height), it will affect $\sigma_n$. Furthermore, since both $\beta$ and $w$ are multiplied by $\mu^n$, the value of $\beta$ also affects $\mu$. Due to the entanglement of variables, the $\chi^2$ minimization shall lead to mutiple solutions.

In the next section, we will show fitting results on the same histogram with two different initial values of parameters.

## Effect of different initial values

In Figure 3.1, the spectral shapes of two different results look similar. As we discussed in the last section, $w$, $\alpha$, $\mu$, Nrml and $\beta$ are highly correlative with one other. One can see from Table 3.1 that the first four parameters do not differ much between the two. However, the other five parameters differ significantly between two cases. For this reason, we introduce the Monte Carlo method to investigate how many local minima could arise from our fittings.

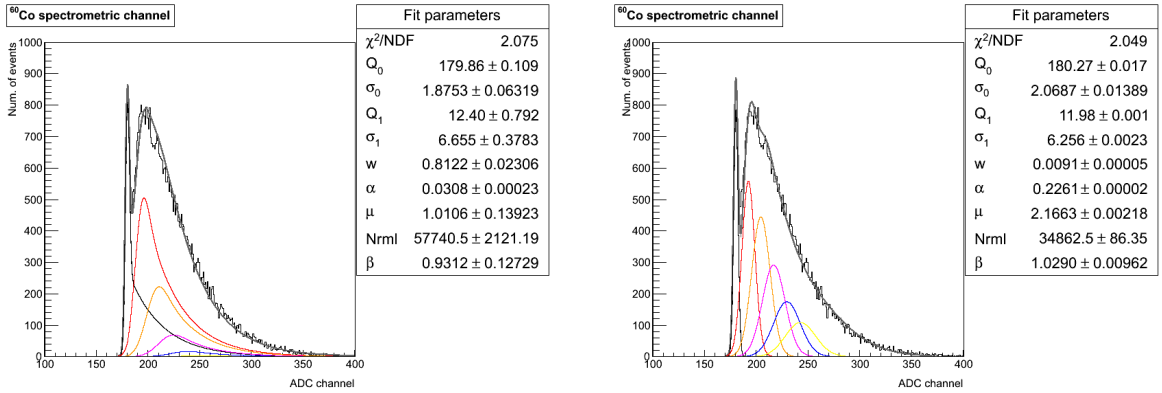


(a) Initial value I

(b) Initial value II

Figure 3.1: $^{60}$Co gamma spectra from QDC CH0. We use different initial conditions to fit the same histogram. The experimental setup is given in Figure 2.3.

| | $Q_0$ | $\sigma_0$ | $Q_1$ | $\sigma_1$ | w | $\alpha$ | $\mu$ | Nrml | $\beta$ | $\chi^2/_{\text{NDF}}$ |
|---|---|---|---|---|---|---|---|---|---|---|
| Initial I | 179.50 | 1.737 | 16.52 | 8.548 | 0.004 | 0.032 | 2.417 | 39107 | 0.2342 | |
| Result I | 179.86 | 1.875 | 12.40 | 6.655 | 0.812 | 0.031 | 1.011 | 57740.5 | 0.93 | 2.08 |
| | ±0.11 | ±0.063 | ±0.79 | ±0.378 | ±0.023 | ±0.0 | ±0.140 | ±2121.2 | ±0.13 | |
| Initial II | 180.27 | 2.068 | 11.96 | 6.280 | 0.009 | 0.230 | 2.000 | 35000.0 | 1.0 | |
| Result II | 180.27 | 2.069 | 11.98 | 6.256 | 0.009 | 0.226 | 2.166 | 34862.5 | 1.03 | 2.05 |
| | ±0.02 | ±0.014 | ±0.0 | ±0.002 | ±0.0 | ±0.0 | ±0.002 | ±86.35 | ±0.01 | |

Table 3.1: The summary of our fitting results. We can see that $w$, $\alpha$, $\mu$, Nrml and $\beta$ are highly correlative with one aother. This confirms our argument in the beginning of this chapter

# Monte Carlo simulation

There are many papers and textbooks which discuss the theory and application of Monte Carlo simulations. Here we only discuss the basic idea. Generally, if one wishes to simulate some physics process in this way, one has to invoke both randomness and probability distribution. The desired physical model must be capable of dealing with random properties. For instance, the emission direction of a uniform weak light source is random, so that the photon distribution on the sphere with fixed radius is also random. However the photon number along the radius attenuates and can be described by some function of distance. This example possesses two essential ingredients we mentioned above: randomness and probability distribution. The key point of Monte Carlo simulation is that one applies random number to fill the probability density function (PDF).

An event could occur only if there is a possibility for such an event to happen. Hence the histogram definitely obeys PDF. In other words, we can simulate the experimental data by PDF and random number generator. The main task is on finding the correct PDF. The details of our simulations are presented in the next few sections.

## Generating data by random number generator

Our random number generator is based on the *Mersenne Twister generator* [3], since it has good random proprieties (period of about $10^{6000}$) and it is fast. The program was taken from ROOT [8] developed by CERN. The algorithm is simple. First, we set up the PDF by fitting to the experimental data. The result is then take as our model. Second, we run the random number generator to reproduce the model such that the output histogram is our new experimental data. Of course this is not the real experimental data, but close enough. To simulate real circumstances, we need to generate many new histograms. We ensure that every histogram is unique. Notice that different random generator has its own algorithm and limitation, *Mersenne Twister generator* has a period of about $10^{6000}$ which is enough for our studies.

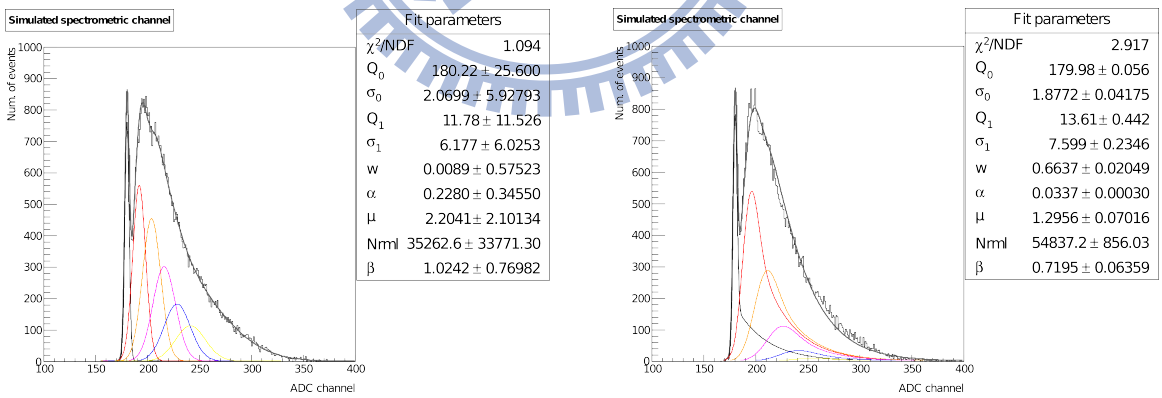


(a) Simulated histogram and fitting I

(b) Simulated histogram and fitting II

Figure 3.2: Simulated QDC CH0 $^{60}$Co gamma spectra. Histograms were generated from Figure 3.1b.

## Identification of local minima

This section deals with the identification of local minima. The model parameters and the initial values used in our fittings are listed in Table 3.2. Notice that we did not include $\beta$ in this list since $\beta$ does not purely come from probability but rather contains geometric information and trigger condition which do not have PDFs.

| | $Q_0$ | $\sigma_0$ | $Q_1$ | $\sigma_1$ | w | $\alpha$ | $\mu$ | Nrml |
|---|---|---|---|---|---|---|---|---|
| Model parameter | 179.5 | 1.7686 | 13.4234 | 6.7379 | 0.7530 | 0.0317 | 1.238 | none |
| Initial I | 179.5 | 1.7686 | 8.4123 | 3.7379 | 0.1253 | 0.2317 | 0.9387 | 50000 |
| Initial II | 179.5 | 1.7686 | 8.4123 | 3.7379 | 0.0953 | 0.2317 | 0.7387 | 50000 |

Table 3.2: List of model parameters and initial values used in our fittings. Notice that $\beta$ is not included in this list.

We generate 2000 histograms for each initial value so there are 2000 groups of fitted parameters at least. We can make a histogram for each parameter. Ideally, if there is no other local minimum, those histograms must be a simple gaussian or delta function. In general there are multiple Gaussians or Gaussian plus delta functions. Figure 3.3 and Figure 3.4 present four histograms. We use several Gaussians to fit each histogram. The complete results are listed in Table 3.3 and Table 3.4.

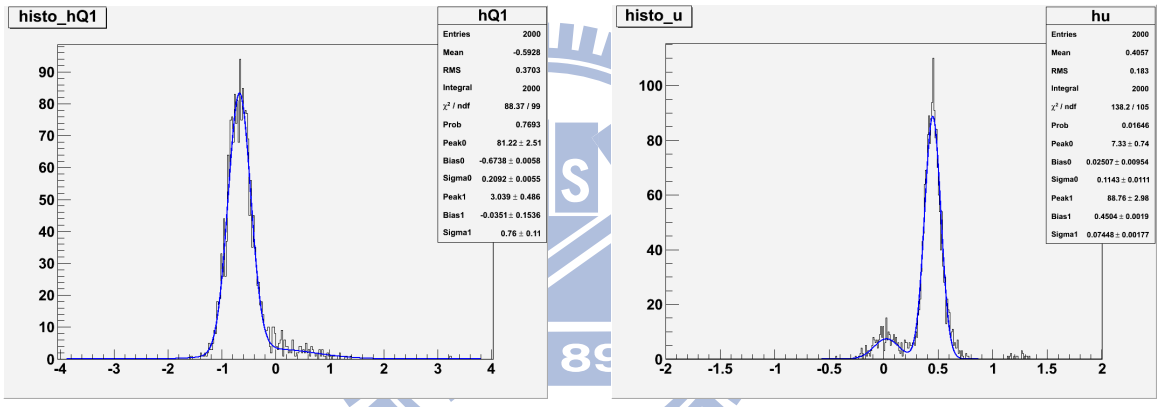


(a) $Q_1$ (b) $\mu$

Figure 3.3: Histogram of $Q_1$ and $\mu$ from Initial I. There are no doubt several local minimums.

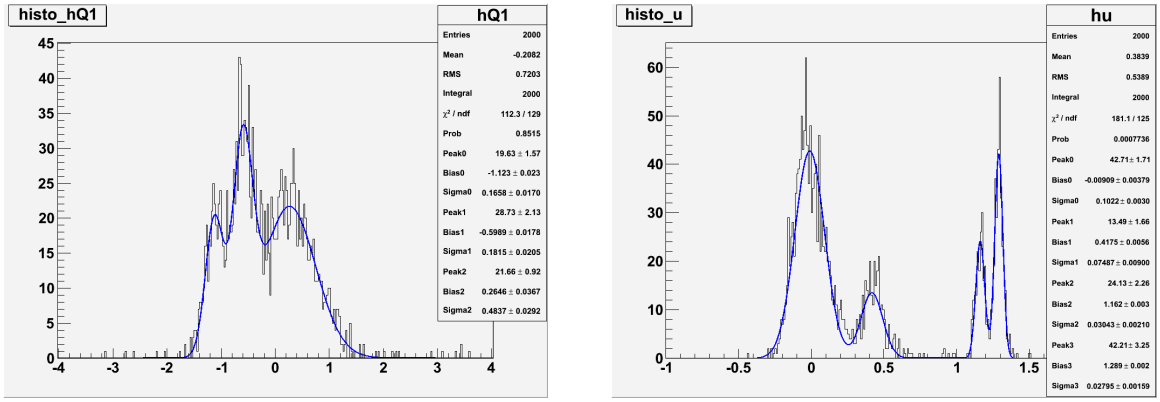


(a) $Q_1$ (b) $\mu$

Figure 3.4: Histogram of $Q_1$ and $\mu$ from Initial II.

| | $Q_0$ | $\sigma_0$ | $Q_1$ | $\sigma_1$ | w | $\alpha$ | $\mu$ | Nrml | $\chi^2/_{\text{NDF}}$ |
|---|---|---|---|---|---|---|---|---|---|
| *1st Gaussian* | | | | | | | | | |
| Mean | 179.52 | 1.7097 | 12.7385 | 6.8759 | 0.5558 | 0.0317 | 1.2631 | 40069 | 1.201 |
| $\sigma$ | 0.0 | 0.0338 | 0.2092 | 0.5074 | 0.0314 | 0.0 | 0.1143 | 57.02 | 0.140 |
| Height | 105.0 | 9.853 | 81.22 | 3.751 | 101.2 | 1600.0 | 7.33 | 7.116 | 26.52 |
| *2nd Gaussian* | | | | | | | | | |
| Mean | 179.63 | | 13.3772 | 8.3919 | 0.7398 | | 1.6884 | 40462 | |
| $\sigma$ | 0.0422 | | 0.76 | 0.4089 | 0.0417 | | 0.0745 | 114.4 | |
| Height | 6.444 | | 3.039 | 41.03 | 11.4 | | 88.76 | 28.04 | |

Table 3.3: Result of Initial I. Mean, $\sigma$, and Height are the parameters of Gaussian fit.

| | $Q_0$ | $\sigma_0$ | $Q_1$ | $\sigma_1$ | w | $\alpha$ | $\mu$ | Nrml | $\chi^2/_{\text{NDF}}$ |
|---|---|---|---|---|---|---|---|---|---|
| *1st Gaussian* | | | | | | | | | |
| Mean | 179.52 | 1.7373 | 12.289 | 6.5756 | 0.0039 | 0.0325 | 1.2289 | 40053 | 0.9772 |
| $\sigma$ | 0.0 | 0.0377 | 0.1658 | 0.3631 | 0.0018 | 0.0 | 0.1022 | 65.04 | 0.0935 |
| Height | 0.0 | 9.037 | 19.63 | 15.62 | 585.4 | 116100 | 42.17 | 33.27 | 22.99 |
| *2nd Gaussian* | | | | | | | | | |
| Mean | | | 12.813 | 7.5047 | 0.5665 | 0.1242 | 1.6555 | 40441 | 1.166 |
| $\sigma$ | | | 0.1815 | 0.9174 | 0.0322 | 0.0050 | 0.0749 | 140.2 | 0.176 |
| Height | | | 28.73 | 8.597 | 14.93 | 46.5 | 13.49 | 3.612 | 8.945 |
| *3rd Gaussian* | | | | | | | | | |
| Mean | | | 13.677 | 10.938 | 0.7530 | | 2.4000 | | |
| $\sigma$ | | | 0.4837 | 0.4445 | 0.0329 | | 0.0304 | | |
| Height | | | 21.66 | 9.97 | 67.29 | | 24.13 | | |
| *4th Gaussian* | | | | | | | | | |
| Mean | | | | | | | 2.5270 | | |
| $\sigma$ | | | | | | | 0.0280 | | |
| Height | | | | | | | 42.21 | | |

Table 3.4: Result of Initial II. Mean, $\sigma$, and Height are the parameters of Gaussian fit.

Comparing Initial values I and II, only initial values of $w$ and $\mu$ are different. Nevertheless, these two cases give totally different results. It seems case II approaches some critical point which has 4 to 5 local minima around. However we expect that there is only one minimun corresponding to the real physics. Other local values are only mathematical. Now the problem is how to filter these unphysical results.

The possible resolution is to fix some parameters which are relatively more stable than others during fittings. We hope that this procedure can reduce the degrees of freedom in the fitting so that other local minima may converge to a single value.

In Table 3.4, $Q_0$, $\sigma_0$ and $\alpha$ are better determined than other variables even though $\alpha$ has two values. Since one probability density of $\alpha$ is much larger than the other, we just treat $\alpha$ as having a single local minimum. After fixing $Q_0$, $\sigma_0$ and $\alpha$, the originally multiple minima solutions now converge to one single solution as shown in Figure. 3.5.

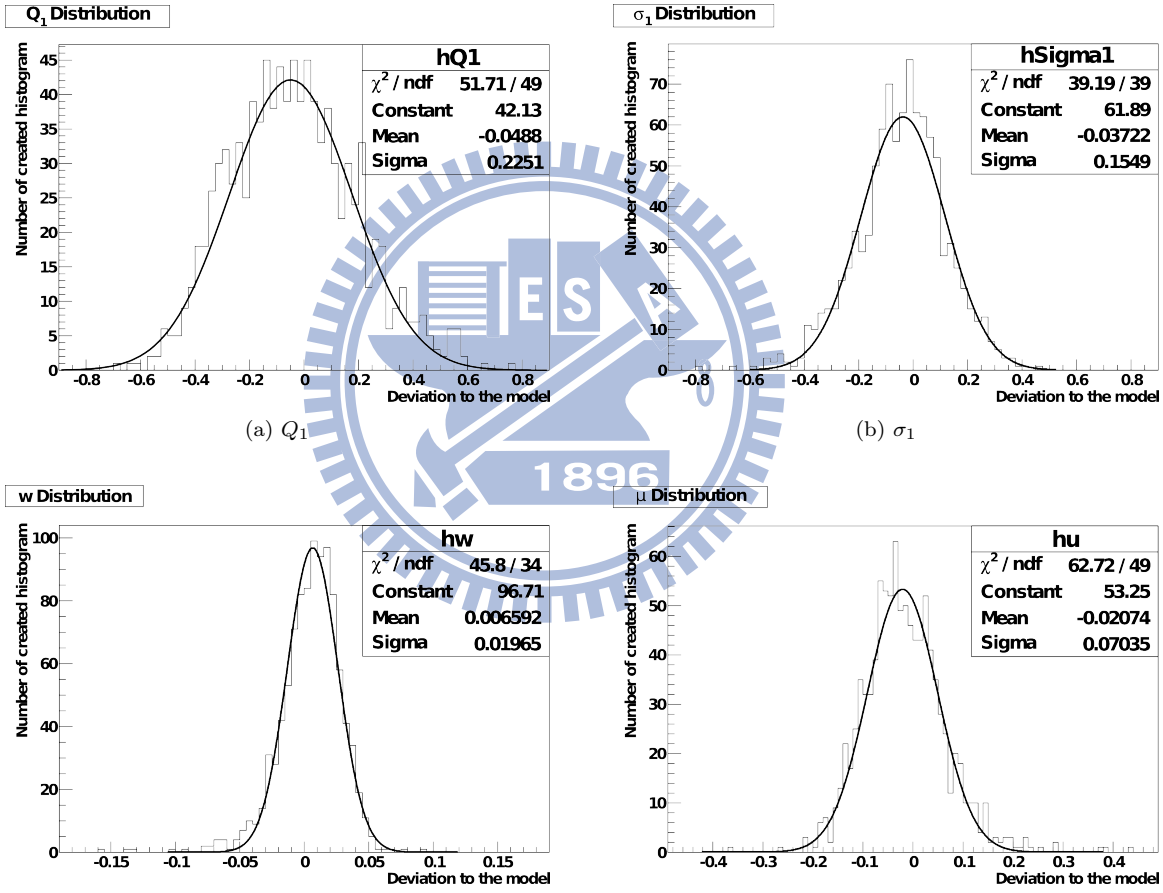


(a) $Q_1$ (b) $\sigma_1$

(c) $w$ (d) $\mu$

Figure 3.5: Monte Carlo result by fixing $Q_0$, $\sigma_0$ and $\alpha$

# Chapter 4

# Summary and Application

## Summary

In Chapter 2, we discussed three main parts of the response function: photoconversion, amplification and background processes. They are described respectively by three approximations which are Poisson distribution, Gaussian distribution and Gaussian plus exponential decay. These approximations were based upon three assumptions.

In *photoconversion and electron collection*, it has been assumed that the event number $N \gg 1$, and the combined probability $p$ for photon collection, photon conversion and electron collection is very small ($p \ll 1$). Under this condition, a binomial distribution approaches to Poisson distribution. The parameter $\mu = Np$ could reflect quantum efficiency of photocathode, electron collection of first dynode, and the source intensity.

During *amplification*, we assumed the number of second emission electrons $K$ on dynode system is not too small ($> 8$ at least), and the probability $\rho$ of electron excited to escape energy at the final dynode remains as a constant. These ensure Gaussian to be a good approximation to the binomial distribution. The parameter $Q_1 = K\rho$ is the average charge at the PMT output when one electron is collected by the first dynode. This parameter can be expressed through the PMT gain coefficient $g$ and elementary charge $e$, as $Q_1 = eg$.

The *background processes* discussed in Chapter 2 mainly include thermionic emission and leakage current. Gaussian and exponential decay describe each process respectively where parameter $w$ is the ratio of pedestal to the thermal effect and $\alpha$ is related to temperature and gain coefficient. In the final section, we presented two set of spectra generated by LED and irradiation respectivrly. We also introduced the coefficient $\beta$ to account for the trigger condition.

In Chapter 3, we first discussed the effect of initial value in the PMT spectrum fitting. There are high correlations between some parameters so that the best-fit parameters are not unique as shown in Table 3.1. This motivates our Monte Carlo study described in Chapter 3. Such a study can check the stability of response function and identify correct physical parameters of PMT.

In next two sections, we shall discuss two applications. The data all came from Aberdeen cosmic ray experiment.

## Monitoring PMT properties

In Aberdeen cosmic ray experiment, electronic modules including high voltage and TDC module are changed at times. The pedestal and the data properties are changed as a result. It is desirable to understand the detector stability after these adjustments are made. Since only the high voltage and TDC are adjusted, so the effects are only reflected in pedestal and background spectrum. Therefore, I focus on monitoring parameters $Q_0$, $\sigma_0$, $Q_1$ and $\sigma_1$. Figure 4.1 shows the result.

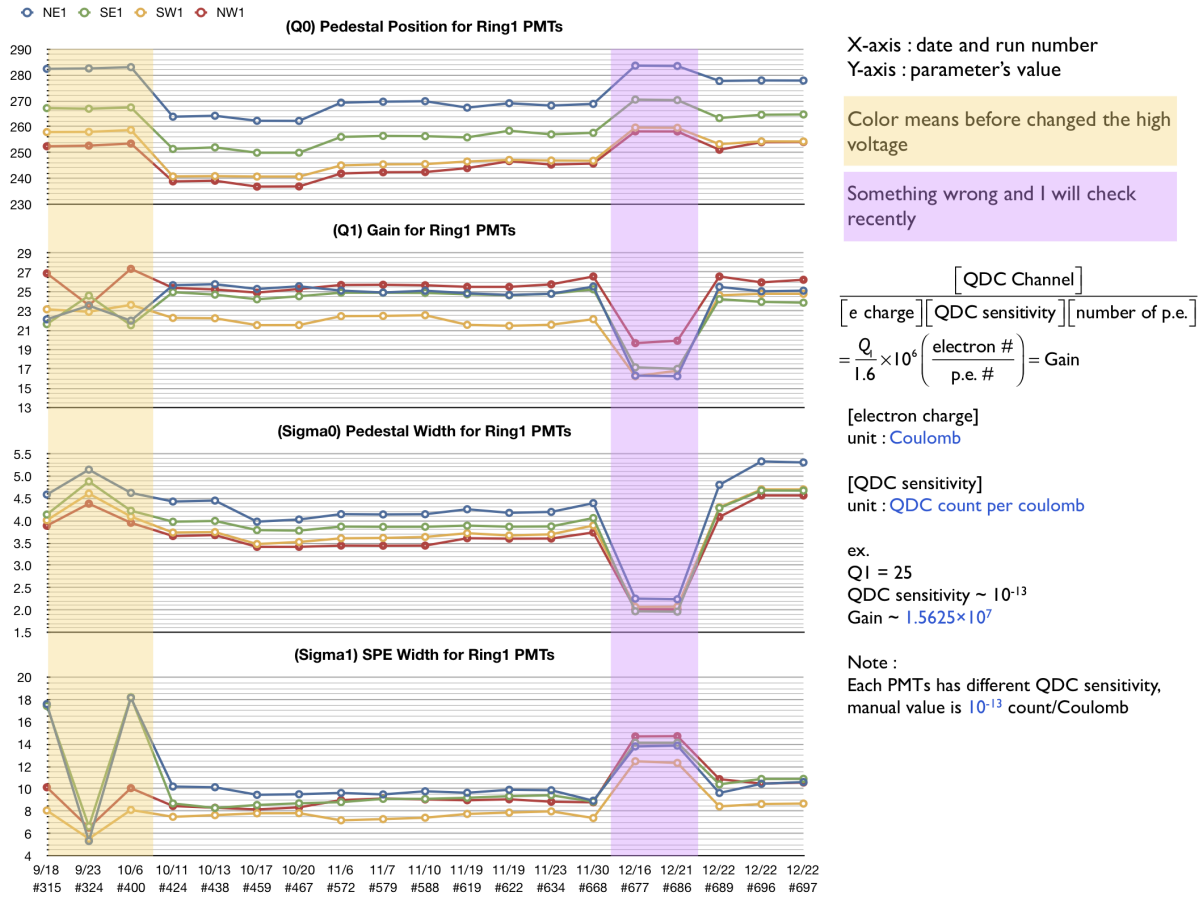


Figure 4.1: The monitoring of PMT parameters $Q_0$, $\sigma_0$, $Q_1$ and $\sigma_1$. There are totally 16 PMTs in the Aberdeen experiment. We only show results of four PMTs situated in the same ring of the detector. Irradiation sources are $^{60}$Co, $^{137}$Cs, and Ambe. Trigger condition is 1 out of 16.

We set up a program to automatically receive the data and fit the spectrum through the response function. Therefore we check the spectrum by our eyes only when the program finds problems such as the purple region in Figure 4.1. These parameters change drastically between Dec. 16th and Dec. 21st. We then checked the ADC spectrum and found that there are two pedestals sticking together. This situation is caused by the width of the time window. After this checking, we performed more calibration on TDC gate and fixed this problem.

## More accurate determination of parameters

Sometimes, the results for the spectrum fitting are quite stable even though the initial value is varied. However the result for the fitting might not be reliable. This could happen due to the sensitivity of $\chi^2$ fitting program to the bulge which is either a statistical fluctuation or some error in the data recording.

We can identify the real problem by Monte Carlo simulation. Since a random generator has its own fluctuation as many histograms are generated and fitted, it is possible to understand whether the bulge is just a DAQ system error, or a part of PDF. If the bulge is just an error in data recording, simulation result could tell us the deviation between the fitted value and real value of a parameter.

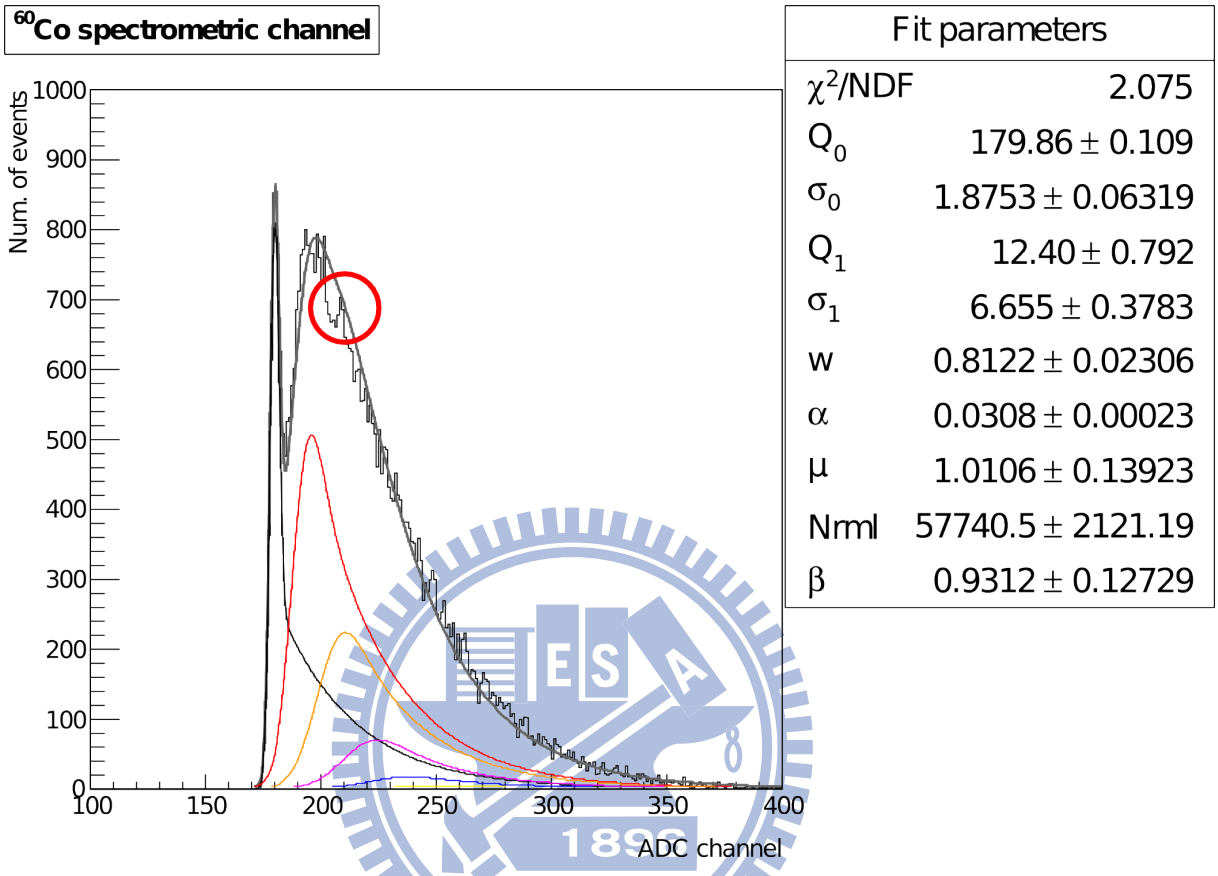


Figure 4.2: The bulge, circled by red line

Actually, the example presented in Chapter 3 is the result of such an analysis. Although we encountered the problem of multiple local minima in the fitting. We have resolved the problem and the results in Figure 3.5 tell us the necessary shifts in parameter values.

# Appendix

## Appendix A : Poisson approximation to the binomial distribution

For convenience in disscussions, let us rewrite (2.1) as

$$\begin{aligned} P(n) &= \frac{N!}{n!(N-n)!}(1-p)^{N-n}p^n \\ &= \frac{N!}{n!(N-n)!}\left(1-\frac{Np}{N}\right)^{N-n}\frac{(Np)^n}{N^n} \\ &= A(n;N)B(n;N,p)\frac{(Np)^n}{n!} \end{aligned} \tag{A.1}$$

where

$$\begin{aligned} A(n;N) &= \frac{N!}{N^n(N-n)!} \\ &= \frac{N(N-1)(N-2)\cdots(N-n+2)(N-n+1)}{N^n} \\ &= (1)\left(1-\frac{1}{N}\right)\left(1-\frac{2}{N}\right)\cdots\left(1-\frac{n-2}{N}\right)\left(1-\frac{n-1}{N}\right) \\ &= \prod_{k=0}^{n-1}\left(1-\frac{k}{N}\right) \end{aligned} \tag{A.2}$$

and $B(n;N,p)$ in the limit $Np/N \to 0$ is expanded as

$$\begin{aligned} B(n;N,p) &= \left(1-\frac{Np}{N}\right)^{N-n} \\ &= 1+\frac{N-n}{1!N}(-Np)+\frac{(N-n)(N-n-1)}{2!N^2}(-Np)^2 \\ &+\cdots+\frac{(N-n)\cdots(3)(2)}{(N-n-1)!N^{N-n-1}}(-Np)^{N-n-1} \\ &+\frac{(N-n)!}{(N-n)!N^{N-n}}(-Np)^{N-n} \\ &= 1+\left(1-\frac{n}{N}\right)\frac{(-Np)}{1!}+\left(1-\frac{n}{N}\right)\left(1-\frac{n+1}{N}\right)\frac{(-Np)^2}{2!} \\ &+\cdots+\left[\left(1-\frac{n}{N}\right)\cdots\left(1-\frac{N-2}{N}\right)\right]\frac{(-Np)^{N-n-1}}{(N-n-1)!} \\ &+\left[\left(1-\frac{n}{N}\right)\cdots\left(1-\frac{N-2}{N}\right)\left(1-\frac{N-1}{N}\right)\right]\frac{(-Np)^{N-n}}{(N-n)!} \\ &= 1+\sum_{l=1}^{N-n}\left[\prod_{s=0}^{l-1}\left(1-\frac{n+s}{N}\right)\right]\frac{(-Np)^l}{(l)!} \end{aligned} \tag{A.3}$$

As mentioned before, if the whole system has been operated for a while, i.e. $N \gg 1$, (A.2), (A.3) and (A.1) can be approximated as follows

$$\begin{aligned}
\lim_{N\gg 1} A(n;N) &\simeq \lim_{N\gg 1} \prod_{k=0}^{n-1} \left(1-\frac{k}{N}\right) \simeq 1 \\
\lim_{N\gg 1} B(n;N,p) &\simeq 1 + \lim_{N\gg 1} \sum_{l=1}^{N-n} \left[\prod_{s=0}^{l-1} \left(1-\frac{n+s}{N}\right)\right] \frac{(-Np)^l}{(l)!} \\
&\simeq 1 + \lim_{N\gg 1} \sum_{l=1}^{N-n} \left[\sim 1\right] \frac{(-Np)^l}{(l)!} \\
\lim_{N\gg 1} P(n) &\simeq \lim_{N\gg 1} A(n;N)B(n;N,p)\frac{(Np)^n}{n!} \\
&\simeq \lim_{N\gg 1} \frac{(Np)^n}{n!}\left[1+\sum_{l=1}^{N-n}\frac{(-Np)^l}{(l)!}\right] \\
&\simeq \lim_{N\gg 1} \frac{(Np)^n}{n!} e^{-Np}
\end{aligned}$$

with $Np = \mu$ as a finite real number, we have

$$P(n;\mu) \simeq \frac{\mu^n}{n!} e^{-\mu} \,, \tag{A.4}$$

which is a Poisson distribution.

## Appendix B : Gaussian approximation to the binomial distribution

We may consider the Gaussian distribution as the limit of a binomial distribution when the number of trials $N \gg 1$ but the probability of a success $p$ is not too small such that $Np \gg 1$. This contracts with the Poisson distribution, which corresponds to the limit $N \gg 1$ with $\mu \equiv Np$ remaining finite. In other words, a Gaussian distribution results when an experiment with a finite probability of success is repeated a large number of times. We now show how this Gaussian limit arises.

The binomial probability function gives the probability of $x$ successes in $N$ trials as

$$G\left(x\right) = \frac{N!}{x!(N-x)!}\left(1-p\right)^{N-x} p^x \,. \tag{B.1}$$

Using the Stirling's asymptotic series

$$n! = \sqrt{2\pi n}\ \ n^n e^{-n}\left(1+\frac{1}{12n}+\frac{1}{288n^2}-\frac{139}{51840n^3}\cdots\right) \,, \tag{B.2}$$

we have, for $n \gg 1$,

$$n! \simeq \sqrt{2\pi n}\ \ n^n e^{-n} \tag{B.3}$$

which is the so called Stirling's approximation. Substituting this result into (B.1), we obtain

$$\begin{aligned}
G\left(x\right) &\simeq \frac{1}{\sqrt{2\pi N}}\left(\frac{x}{N}\right)^{-x-1/2}\left(\frac{N-x}{N}\right) p^x (1-p)^{N-x} \\
&= \frac{1}{\sqrt{2\pi N}} \exp\left[-\left(x+\frac{1}{2}\right)\ln\frac{x}{N} - \left(N-x+\frac{1}{2}\right)\ln\frac{N-x}{N} + x\ln p + (N-x)\ln\left(1-p\right)\right] \\
&= \frac{1}{\sqrt{2\pi}}\frac{1}{\sqrt{Np(1-p)}} \exp\left[-\left(x+\frac{1}{2}\right)\ln\frac{x}{Np} - \left(N-x+\frac{1}{2}\right)\ln\frac{N-x}{N-Np}\right] \,.
\end{aligned} \tag{B.4}$$

By expanding the argument of the exponential in terms of $y = x - Np$, where $1 \ll y \ll Np$ and keeping only the dominant terms, it can be shown that

$$G(x) \simeq \frac{1}{\sqrt{2\pi}} \frac{1}{\sqrt{Np(1-p)}} \exp\left[-Np\left(1+\frac{y}{Np}+\frac{1}{2Np}\right)\ln\left(1+\frac{y}{Np}\right)\right. \tag{B.5}$$
$$\left. -(N-Np)\left(1-\frac{y}{N-Np}+\frac{1}{2(N-Np)}\right)\ln\left(1-\frac{y}{N-Np}\right)\right]$$
$$\simeq \frac{1}{\sqrt{2\pi}} \frac{1}{\sqrt{Np(1-p)}} \exp\left[-Np\left(1+\frac{y}{Np}\right)\ln\left(1+\frac{y}{Np}\right)\right. \tag{B.6}$$
$$\left. -(N-Np)\left(1-\frac{y}{N-Np}\right)\ln\left(1-\frac{y}{N-Np}\right)\right]$$
$$\simeq \frac{1}{\sqrt{2\pi}} \frac{1}{\sqrt{Np(1-p)}} \exp\left[-Np\left(1+\frac{y}{Np}\right)\left(\frac{y}{Np}-\frac{y^2}{2(Np)^2}+\cdots\right)\right. \tag{B.7}$$
$$\left. -(N-Np)\left(1-\frac{y}{N-Np}\right)\left(-\frac{y}{N-Np}-\frac{y^2}{2(N-Np)^2}+\cdots\right)\right]$$
$$\simeq \frac{1}{\sqrt{2\pi}} \frac{1}{\sqrt{Np(1-p)}} \exp\left[-\frac{y^2}{2Np(1-p)}\right] \tag{B.8}$$
$$= \frac{1}{\sqrt{2\pi}} \frac{1}{\sigma} \exp\left[-\frac{(x-Q)^2}{2\sigma^2}\right] \tag{B.9}$$

which is a Gaussian distribution with $Np = Q$ and $\sqrt{Np(1-p)} = \sigma$. Thus we see that the value of the Gaussian probability density function $G(x)$ is a good approximation to the probability of obtaining $x$ successes in N trials. This approximation is actually very good even for relatively small $N$. The probability functions $G(x)$ for the binomial and associated Gaussian distributions are given in Table B.1. It is seen that the Gaussian approximation works well.

| x | Binomial | Gaussian | $\delta(\%)$ |
|---|---|---|---|
| 0 | 0.0167962 | 0.0200051 | 19.10 |
| 1 | 0.0895795 | 0.0816333 | -8.87 |
| 2 | 0.2090190 | 0.1978790 | -5.33 |
| 3 | 0.2786920 | 0.2849280 | 2.24 |
| 4 | 0.2322430 | 0.2437120 | 4.94 |
| 5 | 0.1238630 | 0.1238290 | -0.03 |
| 6 | 0.0412877 | 0.0373745 | -9.48 |
| 7 | 0.0078643 | 0.0067009 | -14.79 |
| 8 | 0.0006554 | 0.0007137 | 8.90 |
| sum | 1 | 0.996776 | |

(a) $N = 8$ and $p = 0.4$

| x | Binomial | Gaussian | $\delta(\%)$ |
|---|---|---|---|
| 0 | 0.0006554 | 0.0007137 | 8.90 |
| 1 | 0.0078643 | 0.0067009 | -14.79 |
| 2 | 0.0412877 | 0.0373745 | -9.48 |
| 3 | 0.1238630 | 0.1238290 | -0.03 |
| 4 | 0.2322430 | 0.2437120 | 4.94 |
| 5 | 0.2786920 | 0.2849280 | 2.24 |
| 6 | 0.2090190 | 0.1978790 | -5.33 |
| 7 | 0.0895795 | 0.0816333 | -8.87 |
| 8 | 0.0167962 | 0.0200051 | 19.11 |
| sum | 1 | 0.996776 | |

(b) $N = 8$ and $p = 0.6$

Table B.1: Gaussian distribution and Binomial distribution

## Appendix C : Convolution of amplification and background

The convolution $G_n\left(x-Q_0\right)\otimes B\left(x\right)$ is given by

$$\begin{aligned} G_n\left(x-Q_0\right)\otimes B\left(x\right) &= \int G_n\left(y-Q_0\right)B\left(x-y\right)\,\mathrm{d}y \\ &= \int_{-\infty}^{\infty}\frac{1-w}{2\pi\sigma_0\sigma_1\sqrt{n}}\exp\left[-\frac{\left(y-Q_n\right)^2}{2n\sigma_1^2}-\frac{\left(x-y\right)^2}{2\sigma_0^2}\right]\mathrm{d}y \\ &+ \int_{-\infty}^{\infty}\frac{w\alpha}{\sigma_1\sqrt{2\pi n}}\Theta\left(x-y\right)\exp\left[-\frac{\left(y-Q_n\right)^2}{2n\sigma_1^2}-\alpha(x-y)\right]\mathrm{d}y\,, \end{aligned} \tag{C.1}$$

where

$$\begin{aligned} Q_n &= Q_0+nQ_1 \\ \sigma_n &= \sqrt{\sigma_0^2+n\sigma_1^2} \\ \Theta\left(z\right) &= \begin{cases} 1 & z\geq 0 \\ -1 & z<0 \end{cases} \end{aligned} \tag{C.2}$$

The whole convolution could be separated into two parts as shown in (C.1). Let us begin with the first integral. Writing the expression in the exponential as perfect squares, we have

$$\begin{aligned} &\int_{-\infty}^{\infty}\frac{1-w}{2\pi\sigma_0\sigma_1\sqrt{n}}\exp\left[-\frac{\left(y-Q_n\right)^2}{2n\sigma_1^2}-\frac{\left(x-y\right)^2}{2\sigma_0^2}\right]\mathrm{d}y \\ &= \int_{-\infty}^{\infty}\frac{1-w}{2\pi\sigma_0\sigma_1\sqrt{n}}\exp\left[-\frac{\left(\sigma_0^2+n\sigma_1^2\right)y^2-2y\left(Q_n\sigma_0^2+n\sigma_1^2x\right)+Q_n^2\sigma_0^2+n\sigma_1^2x^2}{2n\sigma_0^2\sigma_1^2}\right]\mathrm{d}y \\ &= \int_{-\infty}^{\infty}\frac{1-w}{2\pi\sigma_0\sigma_1\sqrt{n}}\exp\left[-\frac{\sigma_n^2}{2n\sigma_0^2\sigma_1^2}\left(y-\frac{Q_n\sigma_0^2+n\sigma_1^2x}{\sigma_n^2}\right)^2\right. \\ &\qquad \left.+\frac{\left(Q_n\sigma_0^2+n\sigma_1^2x\right)^2-Q_n^2\sigma_n^2\sigma_0^2-n\sigma_1^2\sigma_n^2x^2}{2n\sigma_0^2\sigma_1^2\sigma_n^2}\right]\mathrm{d}y \end{aligned} \tag{C.3}$$

The first term inside the exponential in the last equation is nothing but a Gaussian integral

$$\int_{-\infty}^{\infty}\exp\left[-\frac{\sigma_n^2}{2n\sigma_0^2\sigma_1^2}\left(y-\frac{Q_n\sigma_0^2+n\sigma_1^2x}{\sigma_n^2}\right)^2\right]\mathrm{d}y=\frac{\sqrt{2\pi}\sigma_0\sigma_1\sqrt{n}}{\sigma_n} \tag{C.4}$$

Combining and adjusting the last two terms, we have

$$\frac{1-w}{\sigma_n\sqrt{2\pi}}\exp\left[\frac{\left(Q_n\sigma_0^2+n\sigma_1^2x\right)^2-Q_n^2\sigma_n^2\sigma_0^2-n\sigma_1^2\sigma_n^2x^2}{2n\sigma_0^2\sigma_1^2\sigma_n^2}\right] \tag{C.5}$$

Using $\sigma_n^2=\sigma_0^2+n\sigma_1^2$ in the previous equation, we arrive at

$$\begin{aligned} &\frac{1-w}{\sigma_n\sqrt{2\pi}}\exp\left[\frac{\left(Q_n\sigma_0^2+n\sigma_1^2x\right)^2-Q_n^2\sigma_0^4-Q_n^2n\sigma_1^2\sigma_0^2-n\sigma_1^2\sigma_0^2x^2-n^2\sigma_1^4x^2}{2n\sigma_0^2\sigma_1^2\sigma_n^2}\right] \\ &= \frac{1-w}{\sigma_n\sqrt{2\pi}}\exp\left[\frac{2Q_n\sigma_0^2n\sigma_1^2x-Q_n^2n\sigma_1^2\sigma_0^2-n\sigma_1^2\sigma_0^2x^2}{2n\sigma_0^2\sigma_1^2\sigma_n^2}\right] \end{aligned}$$

After simplifications, the first part in the convolution is equal to

$$\frac{1-w}{\sigma_n\sqrt{2\pi}}\exp\left[-\frac{\left(x-Q_n\right)^2}{2\sigma_n^2}\right]\,. \tag{C.6}$$

Next, we calculate the second integral. For thermal emission, the integral range must be considered properly. A signal which can be recorded by DAQ system must be higher than the trigger level (trigger voltage) which is closed to the pedestal. So we assume that $w\alpha \exp(-\alpha x)$ has value only when $x \geq Q_0$. In this case, the integral range is not $(-\infty, \infty)$ anymore but instead $[Q_0, \infty)$, i.e.,

$$\int_{Q_0}^{\infty} \frac{w\alpha}{\sigma_1\sqrt{2\pi n}} \Theta(x-y) \exp\left[-\frac{(y-Q_n)^2}{2n\sigma_1^2} - \alpha(x-y)\right] \mathrm{d}y \tag{C.7}$$

Because $\Theta(x-y) = 0$ for $x - y < 0$, the integral range can be changed again

$$\int_{Q_0}^{x} \frac{w\alpha}{\sigma_1\sqrt{2\pi n}} \exp\left[-\frac{(y-Q_n)^2}{2n\sigma_1^2} - \alpha(x-y)\right] \mathrm{d}y \tag{C.8}$$

Rewriting terms in the exponential into perfect squares, we have

$$\begin{aligned} &\int_{Q_0}^{x} \frac{w\alpha}{\sigma_1\sqrt{2\pi n}} \exp\left[-\frac{y^2 - 2y\left(Q_n + n\sigma_1^2\alpha\right) + Q_n^2 + 2xn\sigma_1^2\alpha}{2n\sigma_1^2}\right] \mathrm{d}y \\ &= \int_{Q_0}^{x} \frac{w\alpha}{\sigma_1\sqrt{2\pi n}} \exp\left[-\frac{\left(y - Q_n - n\sigma_1^2\alpha\right)^2}{2n\sigma_1^2} + \frac{\left(Q_n + n\sigma_1^2\alpha\right)^2 - Q_n^2 - 2xn\sigma_1^2\alpha}{2n\sigma_1^2}\right] \mathrm{d}y \end{aligned} \tag{C.9}$$

Simplifying the above expression, we have

$$\begin{aligned} &\int_{Q_0}^{x} \frac{w\alpha}{\sigma_1\sqrt{2\pi n}} \exp\left[-\frac{\left(y - Q_n - n\sigma_1^2\alpha\right)^2}{2n\sigma_1^2} + \frac{2Q_n n\sigma_1^2\alpha - 2xn\sigma_1^2\alpha + n^2\sigma_1^4\alpha^2}{2n\sigma_1^2}\right] \mathrm{d}y \\ &= \int_{Q_0}^{x} \frac{w\alpha}{\sigma_1\sqrt{2\pi n}} \exp\left[-\frac{\left(y - Q_n - n\sigma_1^2\alpha\right)^2}{2n\sigma_1^2} + Q_n\alpha - x\alpha + \frac{n\sigma_1^2\alpha^2}{2}\right] \mathrm{d}y \\ &= \exp\left[-\alpha\left(x - Q_n - \frac{n\sigma_1^2\alpha}{2}\right)\right] \int_{Q_0}^{x} \frac{w\alpha}{\sigma_1\sqrt{2\pi n}} \exp\left[-\frac{\left(y - Q_n - n\sigma_1^2\alpha\right)^2}{2n\sigma_1^2}\right] \mathrm{d}y \end{aligned} \tag{C.10}$$

The integral part of (C.10) is just two error functions. Let

$$\begin{aligned} t(y) &= \frac{y - Q_n - n\sigma_1^2\alpha}{\sigma_1\sqrt{2n}} \\ \mathrm{d}y &= \sigma_1\sqrt{2n}\,\mathrm{d}t \end{aligned} \tag{C.11}$$

We rewrite (C.10) as

$$\begin{aligned} &\int_{t(Q_0)}^{t(x)} \frac{w\alpha}{\sqrt{\pi}} e^{-t^2}\,\mathrm{d}t \\ &= \frac{w\alpha}{2}\left[\int_0^{t(x)} \frac{2}{\sqrt{\pi}} e^{-t^2}\,\mathrm{d}t - \int_0^{t(Q_0)} \frac{2}{\sqrt{\pi}} e^{-t^2}\,\mathrm{d}t\right] \\ &= \frac{w\alpha}{2}\left[\mathrm{erf}\left(t(x)\right) - \mathrm{erf}\left(t(Q_0)\right)\right] \end{aligned} \tag{C.12}$$

Since the error function is an odd function and $t(Q_0) < 0$, (C.12) can be rewritten as

$$\frac{w\alpha}{2}\left[\mathrm{erf}\left(t(x)\right) + \mathrm{erf}\left(|\,t(Q_0)\,|\right)\right] \tag{C.13}$$

Subsituting (C.11) into (C.13) and replacing the integral part of (C.10) by (C.13), we obtain the following result of convolution

$$\frac{w\alpha}{2} \exp\left[-\alpha\left(x - Q_n - \frac{n\sigma_1^2\alpha}{2}\right)\right] \left[\mathrm{erf}\left(\frac{x - Q_n - n\sigma_1^2\alpha}{\sigma_1\sqrt{2n}}\right) + \mathrm{erf}\left(\frac{|\,Q_0 - Q_n - n\sigma_1^2\alpha\,|}{\sigma_1\sqrt{2n}}\right)\right] \tag{C.14}$$

# Bibliography


[1] E.H. Bellamy *et al.*, Nucl. Instr. and Meth. A **339(3)**, p.468 (1982).

[2] M. Bott-Bodenhausen *et al.*, Nucl. Instr. and Meth. A **315(1 - 3)**, p.236 (1992).

[3] M. Matsumoto and T. Nishimura, ACM Trans. Model. Comput. Simul. **8(1)**, p.3 (1998)

[4] P. de Barbaro *et al.*, ibid., p.317

[5] B. Bencheikh *et al.*, ibid., p.349

[6] R. W. Engstrom, *Photomultiplier Handbook* [Lancaster, PA, USA: RCA, Solid State Division] (1980)

[7] Hamamatsu Photonics K. K., *Photomultiplier Tubes - Basics and Applications* (2006).

[8] ROOT, **Release 5.26.00**, CERN, for more detail, please visit the website: http://root.cern.ch

[9] G. Bellettini *et al.*, *Test of Long Scintillation Counters for Supercolliders*, internal SDC note **SDC-93-552**, submitted to NIM

[10] Solenoidal Detector Collaboration, *SDC Technical Design Report*, **SDC-92-201** (1992)